



# Field-of-view optimized and constrained undistorted single-shot study of intravoxel incoherent motion and diffusion-weighted imaging of the uterus during the menstrual cycle: a prospective study

Xiaodan Li   
Tianzhu Liu   
Jun Chen   
Jiahui Tang   
Wanchun Zhang   
Juan Du   
Lina Li   
Lesheng Huang 

## PURPOSE

This study aimed to compare the variability of the uterus during the menses phase (MP), follicular phase (FP), and luteal phase (LP) of the menstrual cycle using intravoxel incoherent motion diffusion-weighted imaging (IVIM-DWI).

## METHODS

This prospective study was conducted at the Guangdong Provincial Hospital of Traditional Chinese Medicine between January 2022 and January 2023. Women of childbearing age (18–45 years) with appropriate progesterone levels were included in this study. Conventional magnetic resonance imaging and IVIM-DWI scans were performed during the MP, FP, and LP. The differences in IVIM-DWI-derived parameters between these phases were then compared, and the overlap was quantitatively described.

## RESULTS

The apparent diffusion coefficient (ADC) and pure molecular diffusion coefficient ( $D$ ) values from the endometrium, uterine junctional zone (UJZ), and myometrium indicated statistical differences between the MP and FP and the MP and LP (ADC: endometrium, both  $P < 0.001$ ; UJZ,  $P = 0.008$  and  $P < 0.001$ , respectively; myometrium,  $P = 0.033$  and  $P = 0.006$ , respectively;  $D$ : endometrium, both  $P < 0.001$ ; UJZ,  $P = 0.008$  and  $P = 0.006$ , respectively; myometrium,  $P = 0.041$  and  $P = 0.045$ , respectively). The perfusion-related diffusion coefficient ( $D^*$ ) values from the myometrium indicated statistical differences between the FP and MP and the FP and LP ( $D^*$ : myometrium,  $P = 0.049$  and  $P = 0.009$ , respectively). The overlapping endometrium ratios between the MP and FP or LP were lower than 50% in the ADC and  $D$  values (ADC: overlapping of MP and FP: 33.33%, overlapping of MP and LP: 23.33%;  $D$ : overlapping of MP and FP: 40.00%, overlapping of MP and LP: 43.33%).

## CONCLUSION

The ADC and IVIM-derived parameters indicated differences in the uterus in diverse phases of the menstrual cycle, especially in the endometrium in relation to ADC and  $D$  values.

## KEYWORDS

Intravoxel incoherent motion diffusion-weighted imaging, uterus, menses phase, follicular phase, luteal phase, menstrual cycle

From the Department of Gynecology (X.L., J.D., L.L.), Guangdong Hospital of Traditional Chinese Medicine, Zhuhai, China; Department of Radiology (T.L., J.C., J.T., W.Z., L.H. ✉ huanglesheng2008@163.com), Guangdong Hospital of Traditional Chinese Medicine, Zhuhai, China.

Received 09 March 2023; revision requested 14 April 2023; last revision received 21 June 2023; accepted 10 July 2023.



Epub: 09.08.2023

Publication date: 05.09.2023

DOI: 10.4274/dir.2023.232188

You may cite this article as: Li X, Liu T, Chen J, et al. Field-of-view optimized and constrained undistorted single-shot study of intravoxel incoherent motion and diffusion-weighted imaging of the uterus during the menstrual cycle: a prospective study. *Diagn Interv Radiol.* 2023;29(5):656-663.

The observable morphological and signal changes in the uterus on conventional magnetic resonance imaging (MRI) have been clearly described in the literature.<sup>1-3</sup> With the development and application of quantitative MRI sequences, researchers have become interested in the correlation between periodic morphological changes in the uterus and those displayed using quantitative MRI technologies. Kido et al.<sup>4</sup> revealed that the apparent diffusion coefficient (ADC) values of diffusion-weighted imaging (DWI) for the myometrium and endometrium are lower during the menses phase (MP), and the degree of these differences is similar to those reported between malignant and non-malignant tissues. Kılıçkesmez et al.<sup>5</sup> also noted that ADC values increase significantly. Fractional anisotropy values on diffusion tensor imaging tend to decrease in all zones in the secretory phase, with the exception of the uterine junctional zone (UJZ). Recently, Li et al.<sup>6</sup> demonstrated that the T2\* values in the endometrium during the ovulatory phase (OP) and luteal phase (LP) are significantly higher than those in the UJZ and myometrium.

The ADC is a quantitative parameter derived from DWI<sup>7</sup> and has been commonly used and validated as a potential imaging biomarker for evaluating diffuse or focal uterogenic disease<sup>8,9</sup> and monitoring the treatment response of malignant tumors.<sup>10</sup> However, because the ADC represents the degree of mobility of water molecules in tissue, it may not fully account for the tissue characteristics that can be interrogated using DWI techniques.<sup>7,11</sup> However, intravoxel incoherent motion (IVIM) imaging has been approved to help evaluate uterogenic diseases.<sup>9,10,12,13</sup> The IVIM imaging technique is

based on DWI using various  $b$  values,<sup>7</sup> allowing for the separate analysis of two components of random water motion in biological tissues (pure molecular diffusion and perfusion) using the parameters of the pure molecular diffusion coefficient ( $D$ ), perfusion fraction ( $f$ ), and perfusion-related diffusion coefficient ( $D^*$ ).<sup>14</sup> However, the reliability of IVIM imaging for evaluating uterogenic diseases can be influenced by several factors; for instance, the menstrual cycle of women of childbearing age may influence DWI or IVIM parameters.<sup>4</sup> Previous studies have reported DWI or IVIM-derived parameter measurement errors resulting from this issue.<sup>9,13,15-17</sup>

Whether the uterine structure can cause significant changes in IVIM values during the menstrual cycle affects the feasibility, accuracy, and credibility of IVIM clinical diagnoses. Therefore, this study aimed to compare the diagnostic performance of different IVIM-DWI-derived parameters for the phases of the menstrual cycle to explore the degree of changes during the menstrual cycle presented in IVIM-DWI.

## Methods

### Study design and setting

This field-of-view (FOV) optimized and constrained undistorted single-shot (FOCUS) study was a prospective investigation conducted in the Guangdong Provincial Hospital of Traditional Chinese Medicine between January 2022 and January 2023. The FOCUS study protocol has been approved by our institutional Research Ethics Board (approval ZF2022-379) and adhered to the tenets of the Declaration of Helsinki. Signed informed

consent was obtained from each participant. The study flowchart is provided in Figure 1.

### Participants and screening

Healthy female volunteers were recruited and screened in our hospital during the study period. The inclusion criteria were as follows: (1) healthy women aged 18–45 years, (2) premenopausal status with a regular menstrual cycle ( $28 \pm 7$  days), (3) biphasic basal body temperature, (4) no history of gynecologic diseases, and (5) no oral contraceptives or hormone replacement therapy in the previous 12 months. The exclusion criteria were as follows: (1) congenital uterine abnormalities, (2) leiomyoma, (3) history of adenomyosis, (4) abnormal serum hormone levels, (5) pregnancy, (6) age <18 or >45 years, (7) usual contraindications to MRI, or (8) refusal to sign the informed consent form.

To ensure the patients had normal serum hormone levels, we tested the progesterone levels of the recruited patients. We set the progesterone level at <2.84 nmol/L during the LP and >5.8 nmol/L during the MP. If the progesterone level was inconsistent with the menstrual cycle phase, the gynecologist rechecked the participant's progesterone levels during the next menstrual cycle. However, participants were excluded if the results remained inconsistent with the menstrual cycle phases.

After screening with the progesterone test, a color Doppler ultrasound (US) (Voluson S10; GE Healthcare, MA, USA) examination of the female reproductive system was performed to ensure the patient fit the inclusion criteria. The US examination included the following: 1) exclusion of lesions in the

#### Main points

- Statistical differences between the menses phase (MP) and follicular phase (FP)/luteal phase (LP) were identified in the endometrium, uterine junctional zone, and myometrium in relation to apparent diffusion coefficient ( $D$ ) and pure molecular  $D$  values in intravoxel incoherent motion diffusion-weighted imaging (IVIM-DWI).
- Statistical differences in perfusion-related  $D$  values were identified between the LP and MP/FP in the myometrium through IVIM-DWI.
- The differences in the uterine structure observed through IVIM-DWI can provide experimental evidence for the inclusion/exclusion criteria or layered analysis in future IVIM-DWI uterus studies in women of childbearing age.

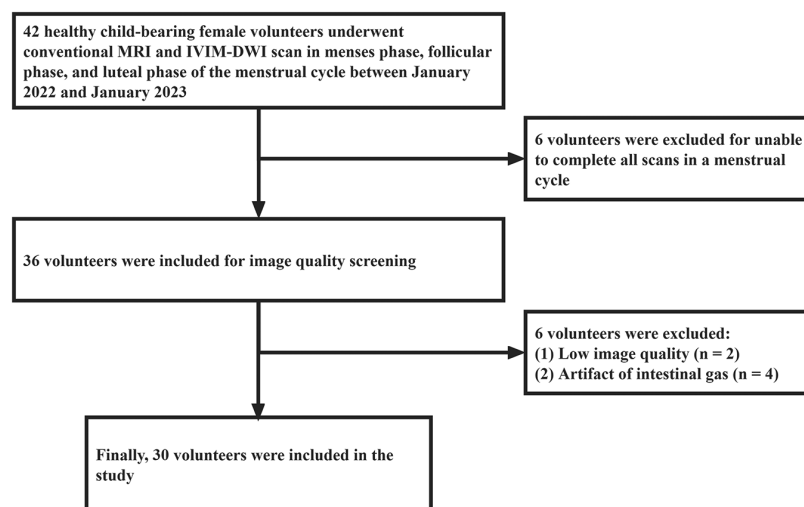


**Figure 1.** Flowchart of the screening process of female volunteers of childbearing age. MRI, magnetic resonance imaging; IVIM, intravoxel incoherent motion diffusion; DWI, diffusion-weighted imaging.

uterus, bilateral fallopian tubes, and ovaries; 2) assessment of the size and position of the uterus; 3) evaluation of the uniformity of the myometrium layer echo; 4) measurement of endometrial thickness; and 5) analysis of uterine blood flow signals.

### Magnetic resonance imaging examination

All participants underwent repeated MRIs over multiple time points during the menstrual cycle. Time point one ( $T_1$ ) was from days 1 to 4 of the menstrual cycle, time point two ( $T_2$ ) was from days 7 to 12, and time point three ( $T_3$ ) was from days 16 to 24;  $T_1$ ,  $T_2$ , and  $T_3$  represent the MP, follicular phase (FP), and LP, respectively. Because the precise time window of the OP is too short to measure accurately, we did not examine the uterus for OP.

The MRI examinations were performed using a 3.0-T scanner (Signa Discovery 750 w; GE Healthcare) with a 16-channel abdominal coil. Participants were required to undertake bowel preparation, including a low-fiber diet for one day, an 8-hour fast before the test, and an enema with 500 mL of saline 30 min before the MRI. For all participants, the following five standard sequences were performed: (1) sagittal T2-weighted short T1 inversion recovery (STIR) sequence, (2) axial T1-weighted turbo spin-echo sequence, (3) axial STIR sequence, (4) sagittal FOCUS DWI sequence, and (5) sagittal FOCUS IVIM sequence.

An IVIM-DWI using a FOCUS protocol was performed on all participants in the sagittal plane in a supine position. The scan range covered the whole uterus and extended 5–8 cm beyond the distal border of the uterus. Spatial saturation bands were applied to remove the signal from the overlying fat and nearby tissues. In addition, the following 12  $b$  values were applied: 0, 25, 50, 75, 100, 150, 200, 300, 400, 500, 600, and 800  $s/mm^2$ .

Participants were asked to breathe freely during the examination, resulting in the following: average repetition time: 3007 ms; average echo time: 69 ms; slice thickness: 4 mm; inter-slice gap: 1 mm; matrix: 48 × 48; FOV: 240 × 240 mm; number of excitations = 2; number of slices = 16–20 (based on the size of the uterus). Two  $b$  values (0 and 800  $s/mm^2$ ) were applied to the FOCUS DWI sequence, and diffusion-weighted gradients were applied in three orthogonal directions. The remaining scan parameters were consistent with the FOCUS IVIM sequence. The total scan time was approximately 30–35 min.

### Image analysis

The IVIM parameters and ADC maps were generated and calculated using FuncTool (GE AW4.6 advantage; GE Healthcare). A quantitative analysis of DWI data was performed using mono-exponential and bi-exponential models for IVIM data. The ADCs were calculated through the mono-exponential linear fitting technique using the following equation:<sup>18</sup>

$$\frac{S(b)}{S_0} = \exp(-b \times ADC),$$

where  $S(b)$  corresponds to the mean signal intensity at a given  $b$  value and  $S_0$  is the mean signal intensity at  $b = 0 s/mm^2$ .

For the bi-exponential model, the IVIM-derived parameters were calculated using the following equation:<sup>19</sup>

$$\frac{S(b)}{S_0} = [(1 - f) \times \exp(-b \times D)] + [f \times \exp(-b \times D^*)],$$

where  $D$  is pure water diffusion,  $D^*$  represents pseudo diffusion, and  $f$  values are the intravascular water fractions in a selected area. The values were calculated using  $b$  values >200 and <200  $s/mm^2$ , respectively.

The quality of the IVIM, DWI, and routine T1-weighted and T2-weighted images was evaluated by a single examiner (JC) with 17 years abdominal MRI experience. Moreover, a trained examiner (LT) with ten years experience in female reproductive system MRI-based diagnosis post-processed all qualified images and then measured the study param-

eters quantitatively at the post-processing workstation. The examiner was blinded to the participants' age, menstrual cycle phases, body mass index (BMI), and previous reproductive history.

To minimize measurement errors, three non-overlapping regions of interest (ROIs) were determined, avoiding visible vessels, uterine borders, and artifacts: (1) the endometrium, anterior, and posterior region of the UJZ; (2) the anterior, posterior, and fundus of the myometrium; and (3) the anterior and posterior region of the cervical muscularis. The size of each ROI was adjusted according to the measurable range of the anatomical structure [endometrium: 15 (mean) and 12–20  $mm^2$  (range); UJZ: 8 (mean) and 5–12  $mm^2$  (range); myometrium and cervical muscularis: 20 (mean) and 15–25  $mm^2$  (range)], and the position was maintained on the different parametric maps (Figure 2). The mean ADC,  $D$ ,  $D^*$ , and  $f$  values for each anatomical structure (endometrium, UJZ, myometrium, and cervical muscularis) were obtained by averaging the measurements in the ROIs (Figure 2).

### Statistical analysis

Statistical analyses were performed using SPSS version 26.0 (Chicago, IL, USA). We tested continuous variables for normal distribution using the Kolmogorov–Smirnov test. Variables with a normal distribution were expressed as mean ± standard deviation, those with a non-normal distribution were expressed as the median (minimum–maximum), and categorical variables were presented as frequencies with percentages. A chi-squared test was applied to analyze

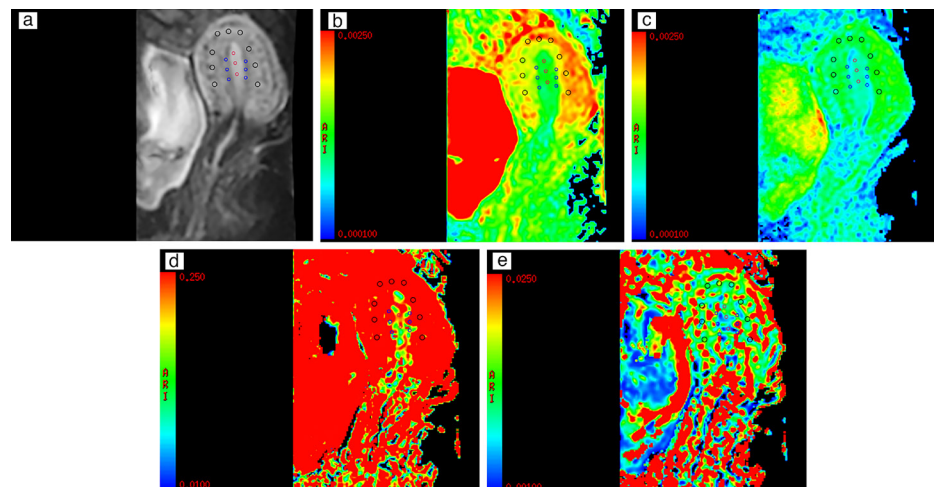


**Figure 2.** A 25-year-old healthy female participant in the follicular phase. (a) Sagittal view of a diffusion-weighted image with  $b: 0 s/mm^2$ ; (b) apparent diffusion coefficient map; (c) pure molecular diffusion coefficient map; (d) perfusion-related diffusion coefficient map; (e) perfusion fraction map. Examiner-measured endometrium (red circles, a-e), uterine junctional zone (blue circles, a-e), and myometrium (black circles, a-e) in sagittal view.

categorical variables. Based on the variable distribution and homogeneity of variance, a Student's t-test or Mann-Whitney U test was applied to compare the differences in each DWI or IVIM-derived parameter between the three menstrual cycle phases.

To quantitatively describe the overlapping conditions and differentiation in menstrual cycle phases in relation to IVIM-DWI parameters, we divided the continuous data into intervals, and based on the order of magnitudes, we set the interval ranges as follows: (1) the interval ranges of the ADC and  $D$  were  $0.10 \times 10^{-3}$  (e.g., an ADC interval of  $1.20 \times 10^{-3}$  mm<sup>2</sup>/s including data between  $1.15 \times 10^{-3}$  and  $1.25 \times 10^{-3}$  mm<sup>2</sup>/s ( $1.15 \times 10^{-3}$  mm<sup>2</sup>/s  $\leq x < 1.25 \times 10^{-3}$  mm<sup>2</sup>/s); (2) the interval range of  $D^*$  was  $10 \times 10^{-3}$  mm<sup>2</sup>/s; (3) the interval range of  $f$  was 10.00%. After the data intervals were processed, the frequencies of each interval were calculated; overlapping intervals and overlapping ratios between the phases were then calculated within the range of a 95% confidence interval of the intervals. In this study, clinical differences were identified when overlapping ratios between the phases were  $< 50\%$ , and  $P < 0.05$  was considered statistically significant.

## Results

### Characteristics of participants

We recruited 42 healthy female volunteers of childbearing age (18–45 years). Six participants (14.29%) were unable to complete all the scans in a menstrual cycle, two (4.76%) were excluded because of low image quality in screening, and four (9.52%) were excluded because they had artifacts in the form of intestinal gas. Finally, 30 participants (71.4%), with a mean age of  $29.33 \pm 5.76$  years, were included in this study.

The characteristics of the participants are summarized in Table 1. Seventeen participants (56.67%) had not given birth, seven (23.33%) had one child (two cesareans and five eutocia), and six (20.00%) had two children (four cesareans and eight eutocia); menstrual cycles were 30 days (26–35 days). The mean BMI of the participants was  $20.48 \pm 2.55$  kg/m<sup>2</sup>, and none were obese.

### Endometrium

During the menstrual cycle, the endometrium ADC and  $D$  values indicated a statistically significant decrease in the MP compared with the FP and LP (ADC: both  $P < 0.001$ ,  $D$ : both  $P < 0.001$ ). However, no statistical differences among the MP, FP,

and LP were identified in the endometrium  $D^*$  and  $f$  values ( $D^*$ : MP and FP:  $P = 0.171$ , MP and LP:  $P = 0.061$ , FP and LP:  $P = 0.753$ ;  $f$ : MP and FP:  $P = 0.770$ , MP and LP:  $P = 0.651$ , LP and FP:  $P = 0.410$ ) (Tables 2, 3 and Figure 3).

The endometrium exhibited low overlapping ratios between the MP and FP/LP in the ADC (MP and FP: 33.33%; MP and LP: 23.33%) and  $D$  (MP and FP: 40.00%; MP and LP: 43.33%), and the overlapping intervals between the MP, FP, and LP in the ADC (MP and FP:  $1.0\text{--}1.3 \times 10^{-3}$  mm<sup>2</sup>/s; MP and LP:  $1.0\text{--}1.3 \times 10^{-3}$  mm<sup>2</sup>/s) and  $D$  (MP and FP:  $0.6\text{--}1.1 \times 10^{-3}$

mm<sup>2</sup>/s; MP and LP:  $0.7\text{--}1.1 \times 10^{-3}$  mm<sup>2</sup>/s) were less than those between the FP and LP (FP and LP: ADC,  $1.0\text{--}1.6 \times 10^{-3}$  mm<sup>2</sup>/s;  $D$ ,  $0.7\text{--}1.4 \times 10^{-3}$  mm<sup>2</sup>/s) (Table 4, Figure 4).

### Uterine junction zone

During the menstrual cycle, the UJZ ADC and  $D$  values demonstrated a statistically significant decrease in the MP compared with the FP and LP (ADC: MP and FP,  $P = 0.008$ , and MP and LP,  $P < 0.001$ ;  $D$ : MP and FP,  $P = 0.008$ , MP and LP:  $P = 0.006$ ). However, no statistical difference was identified among the MP, FP, and LP in the UJZ  $D^*$  and  $f$  values ( $D^*$ : MP and FP,  $P = 0.753$ , MP and LP,  $P = 0.703$ , LP and FP,

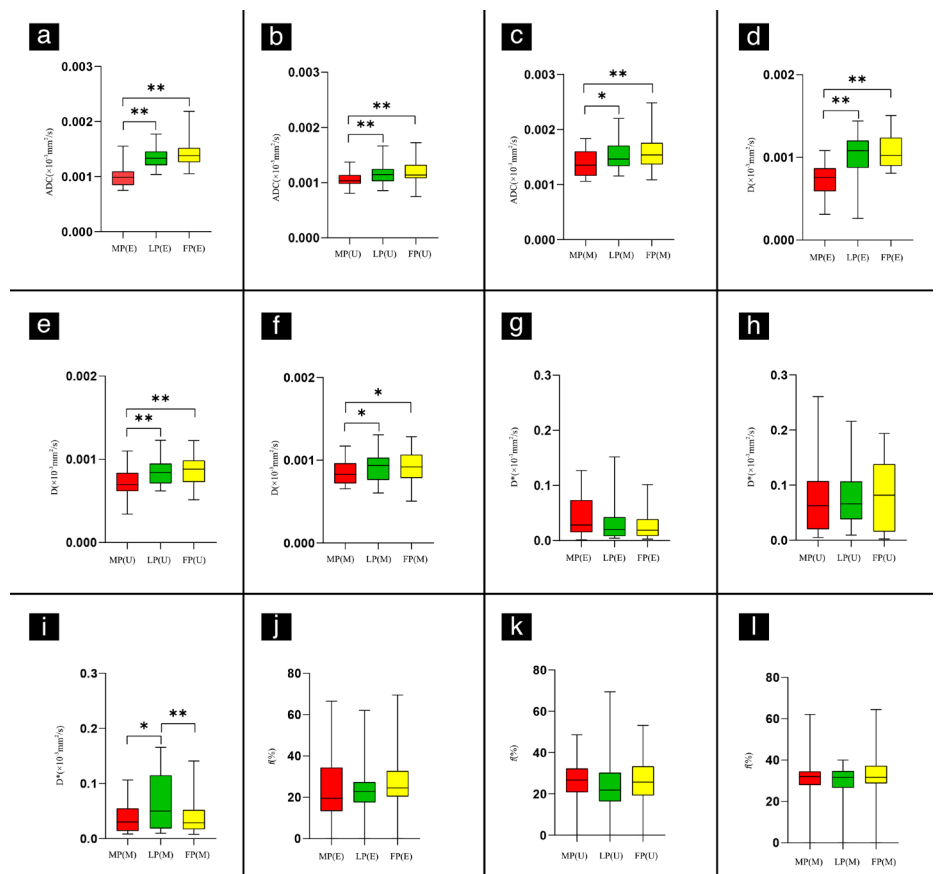


**Figure 3.** Box plots of different phases [menses (MP), luteal (LP), and follicular (FP)] in the endometrium, uterine junction zone (UJZ), and myometrium using parameters derived from intravoxel incoherent motion diffusion-weighted imaging. Apparent diffusion coefficient and pure molecular diffusion coefficient values in the endometrium, UJZ, and myometrium, revealing differences between the MP and LP/FP (a–f,  $P < 0.05$ ), especially in the endometrium (a, d,  $P < 0.001$  all). Perfusion-related diffusion coefficient values in the myometrium, which differ for LP and MP/FP (f,  $P < 0.05$ ) (E = endometrium; U = UJZ; M = myometrium).

**Table 1.** Demographic data of participants

Characteristics	Participants (n = 30)
Age (years), mean $\pm$ standard deviation	$29.33 \pm 5.76$
Procreation (N/O/T)	17/7/6 (56.67%/23.33%/20.00%)
Birth mode (none/cesarean/eutocia)	17/6/13 (47.22%/16.67%/36.11%)
Menstrual cycle (days), median (minimum–maximum)	30 (26–35)
BMI (kg/m <sup>2</sup> )	$20.48 \pm 2.55$

N, none; O, one; T, two; BMI, body mass index.

$P = 0.873$ ;  $f$ : MP and FP,  $P = 0.370$ , MP and LP,  $P = 0.794$ , LP and FP,  $P = 0.256$ ) (Tables 2, 3 and Figure 3).

The UJZ exhibited high overlapping ratios (60.00%–80.00%) and no apparent differences in the overlapping interval between phases in the IVIM-DWI-derived parameters (Table 4, Figure 4).

## Myometrium

During the menstrual cycle, the myometrium ADC and  $D$  values demonstrated a statistically significant decrease in the MP compared with the FP and LP (ADC: MP and FP,  $P = 0.033$ , MP and LP,  $P = 0.006$ ;  $D$ : MP and FP,  $P = 0.041$ , MP and LP,  $P = 0.045$ ) but no statistically significant change in the LP and FP (ADC: LP and FP,  $P = 0.168$ ;  $D$ : LP and FP,

$P = 0.624$ ). However,  $D^*$  values indicated a statistically significant increase in the FP compared with the MP and LP (FP and MP,  $P = 0.049$ ; FP and LP,  $P = 0.009$ ). Moreover, the myometrium  $f$  values indicated no statistical difference in the MP, FP, and LP (MP and FP,  $P = 0.284$ ; MP and LP,  $P = 0.997$ ; LP and FP,  $P = 0.282$ ) (Tables 2, 3 and Figure 3).

The myometrium had highly overlapping ratios (60.00%–86.67%) and no apparent differences in overlapping intervals between phases in the IVIM-DWI parameters (Table 4, Figure 4).

## Discussion

The endometrium is divided into basal and functional layers, with changes to the endometrium occurring in the functional layer.<sup>20</sup> The thickness of the endometrium is approximately 1–4, 12–13, and 16–18 mm in the MP, LP, and FP, respectively.<sup>21</sup> During the MP, changes in phenotype involve the release of proinflammatory cytokines, chemokines, and matrix metalloproteinases, leading to the collapse of the shallow endometrial layer, focal bleeding, and menstrual shedding.<sup>22</sup> Conversely, mesenchyme cells have relatively high or high edema and

Value of IVIM-DWI parameter	ADC ( $\times 10^{-3}$ mm <sup>2</sup> /s)	$D$ ( $\times 10^{-3}$ mm <sup>2</sup> /s)	$D^*$ ( $\times 10^{-3}$ mm <sup>2</sup> /s)	$f$ (%)
<b>Endometrium</b>				
MP of endometrium	0.98 $\pm$ 0.18	0.74 $\pm$ 0.19	28.30 (1.51–127.23)	19.80 (4.59–66.47)
LP of endometrium	1.34 $\pm$ 0.18	1.08 $\pm$ 0.24	20.07 (4.41–151.90)	23.47 (6.14–62.10)
FP of endometrium	1.42 $\pm$ 0.25	1.08 $\pm$ 0.21	18.97 (2.82–101.63)	28.00 $\pm$ 12.37
<b>UJZ</b>				
MP of UJZ	1.06 $\pm$ 0.14	0.73 $\pm$ 0.17	73.12 $\pm$ 60.28	27.87 $\pm$ 9.67
LP of UJZ	1.15 $\pm$ 0.17	0.85 $\pm$ 0.17	77.75 $\pm$ 51.65	24.79 $\pm$ 12.30
FP of UJZ	1.14 (0.75–1.72)	0.85 $\pm$ 0.17	80.16 $\pm$ 64.69	27.08 $\pm$ 10.61
<b>Myometrium</b>				
MP of myometrium	1.40 $\pm$ 0.25	0.85 $\pm$ 0.14	30.16 (8.39–106.26)	32.33 (17.97–62.10)
LP of myometrium	1.52 $\pm$ 0.25	0.90 $\pm$ 0.17	50.03 (9.60–165.53)	30.91 $\pm$ 5.53
FP of myometrium	1.58 $\pm$ 0.30	0.92 $\pm$ 0.20	28.63 (7.68–140.80)	31.87 (13.90–64.40)

IVIM-DWI, intravoxel incoherent motion diffusion-weighted imaging; ADC, apparent diffusion coefficient;  $D$ , pure molecular diffusion coefficient;  $D^*$ , perfusion-related diffusion coefficient;  $f$ , perfusion fraction; MP, menses phase; FP, follicular phase; LP, luteal phase; UJZ, uterine junctional zone.

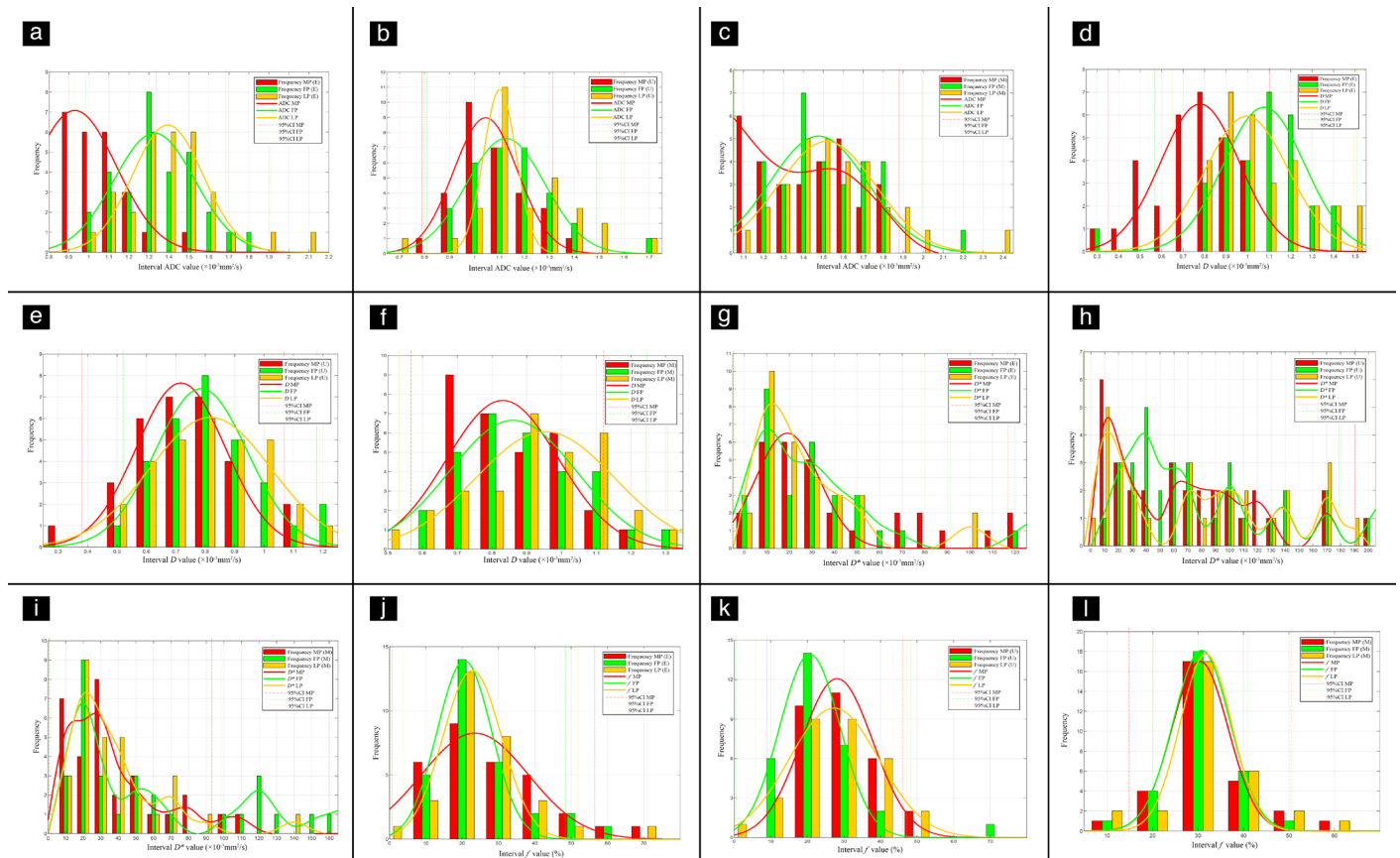


**Figure 4.** (a–l) Histogram and fitted curve graph of the overlapping conditions. MP, menses phase; FP, follicular phase; LP, luteal phase; ADC, apparent diffusion coefficient, CI, confidence interval.

are lost during spiral arteriole hyperplasia in the LP and FP.<sup>23-25</sup> In this study, we found that lower ADC and *D* values produced offset fitted curves for the MP and smaller overlapping intervals and lower overlapping ratios in the MP and LP/FP in terms of ADC and *D* values, consistent with endometrial physiology. These findings support the rationale that water molecule diffusion in endometrial cells decreases with the shedding of edematous mesenchyme cells in the functional layer.

After the demise of the corpus luteum and progesterone level decrease, UJZ-dominated and myometrium-involved antero- (from the fundus of the uterus to the cervix) contractility increases with an increase in uterine contraction (UC) breadth, frequency, and resting tone. Unlike retrograde contraction during the LP and FP, antero- (from the fundus of the uterus to the cervix) contractility increases in intensity and frequency to empty the uterine contents.<sup>26</sup> UCs are often felt by women during the MP, sometimes experienced as an aching feeling (dysmen-

orrhoea). Furthermore, UC can cause the endometrium to be drawn into the myometrium, leading to endometriosis.<sup>27</sup> Substantial constriction from the UJZ and myometrium may cause the blood to flow out of the muscular layer, with the decrease in blood volume leading to a decrease in water content. Contraction forces the smooth muscle cells to tighten, which may be why the ADC and *D* values reduce during the MP.<sup>28</sup> The myometrium exhibits decreased signal intensity under conventional MRI, and the UJZ is unclear in T2-weighted images during the MP. However, the myometrium has higher signal intensity and the UJZ architecture is clearly defined during the LP.<sup>1</sup> This phenomenon may indirectly indicate that the myometrium and UJZ have tight myometrium structures. UC during the MP reduces water molecules in tissues. In the present study, although the UJZ and myometrium ratios overlapped by more than 50%, the fitted curve and highest frequencies were also offset to the left for lower ADC and *D* values in the MP (Figure 4), similar to the endometrium.

Tan et al.<sup>29</sup> reported that the pulsatility index peaked on the day of the luteinizing hormone surge in the dominant and non-dominant uterine arteries during the FP. The dominant uterine artery pulsatility index then declined from the peak to a low level in the mid-LP. The hemodynamic changes correlated with the variations in serum estradiol and progesterone concentrations. Fur-

**Table 3.** *P* value of the parameter comparison between different menstrual cycle phases in the endometrium, UJZ, and myometrium

<i>P</i> value of IVIM-DWI parameter	ADC	<i>D</i>	<i>D</i> *	<i>f</i>
<b>Endometrium</b>				
MP vs. FP	<0.001	<0.001	0.171	0.770
MP vs. LP	<0.001	<0.001	0.061	0.651
LP vs. FP	0.133	0.668	0.753	0.410
<b>UJZ</b>				
MP vs. FP	0.008	0.008	0.753	0.370
MP vs. LP	<0.001	0.006	0.703	0.794
LP vs. FP	0.203	0.954	0.873	0.256
<b>Myometrium</b>				
MP vs. FP	0.033	0.041	0.049	0.284
MP vs. LP	0.006	0.045	0.980	0.997
LP vs. FP	0.168	0.624	0.009	0.282

IVIM-DWI, intravoxel incoherent motion diffusion-weighted imaging; ADC, apparent diffusion coefficient; *D*, pure molecular diffusion coefficient; *D*\*, perfusion-related diffusion coefficient; *f*, perfusion fraction; MP, menses phase; FP, follicular phase; LP, luteal phase; UJZ, uterine junction zone.

**Table 4.** Overlapping conditions during different phases of the menstrual cycle based on IVIM-DWI parameters and uterine structure

	Overlapping interval of M (ADC, <i>D</i> , <i>D</i> *: ×10 <sup>-3</sup> mm <sup>2</sup> /s; <i>f</i> : %)	Overlapping interval of UJZ (ADC, <i>D</i> , <i>D</i> *: ×10 <sup>-3</sup> mm <sup>2</sup> /s; <i>f</i> : %)	Overlapping interval of E (ADC, <i>D</i> , <i>D</i> *: ×10 <sup>-3</sup> mm <sup>2</sup> /s; <i>f</i> : %)	Overlapping ratios of M (%)	Overlapping ratios of UJZ (%)	Overlapping ratios of E (%)
<b>ADC</b>						
MP vs. FP	1.2–1.8	0.9–1.3	1.0–1.3	73.33	76.67	33.33
MP vs. LP	1.2–1.8	0.9–1.3	1.0–1.3	70.00	70.00	23.33
FP vs. LP	1.2–1.8	0.9–1.4	1.0–1.6	70.00	66.67	76.67
<b><i>D</i></b>						
MP vs. FP	0.7–1.1	0.6–1.0	0.6–1.1	83.33	73.33	40.00
MP vs. LP	0.7–1.1	0.6–1.0	0.7–1.1	60.00	63.33	43.33
FP vs. LP	0.5–1.2	0.6–1.1	0.7–1.4	66.67	80.00	76.67
<b><i>D</i>*</b>						
MP vs. FP	10–70	10–130	10–70	53.33	60.00	66.67
MP vs. LP	10–70	10–140	10–50	60.00	73.33	70.00
FP vs. LP	10–70	10–140	0–50	66.67	63.33	80.00
<b><i>f</i></b>						
MP vs. FP	20–40	20–40	10–40	86.67	63.33	73.33
MP vs. LP	20–50	20–40	10–50	80.00	80.00	73.33
FP vs. LP	20–40	10–40	10–40	86.67	70.00	73.33

IVIM-DWI, intravoxel incoherent motion diffusion-weighted imaging; ADC, apparent diffusion coefficient; *D*, pure molecular diffusion coefficient; *D*\*, perfusion-related diffusion coefficient; *f*, perfusion fraction; M, myometrium; U, uterine junctional zone; E, endometrium; MP, menses phase; FP, follicular phase; LP, luteal phase.

thermore, Raine-Fenning et al.<sup>30</sup> noted that both the endometrial and sub-endometrial vascularization index and vascularization flow index increased during the FP, peaking 3 days before ovulation before decreasing to the lowest point 5 days post-ovulation. Similar to Tan et al.<sup>29</sup>, our study revealed that  $D^*$  values, which denote the level of the tissue body fluid or blood perfusion, were high during the FP; however, no obvious differences were observed in the histogram and fitted curve graph. This may be due to the low sample size and discrete interval of  $D^*$  values. Differences in the myometrium were also identified during the menstrual cycle in the T2-weighted MRI scans.<sup>1</sup> The UJZ did not exhibit a similar variation in our study, possibly due to the priority levels of the uterine artery blood supply.

IVIM imaging is a new method for probing tissue perfusion and diffusion without using a contrast agent and has been applied in clinical studies of uterus lesions.<sup>13,15,16,31</sup> However, most studies<sup>13,15,31</sup> fail to explain or describe menstrual cycle details. From the results of our study, the different phases of the menstrual cycle demonstrated significant differences in IVIM-derived parameters, especially in the endometrium for low overlapping ratios between phases, which could undermine the credibility of studies. Therefore, based on the rigor of clinical research, we suggest that studies of the uterus and IVIM should be conducted during the same phase of the menstrual cycle, if possible.

This study has some strengths. First, we presented explainable results for DWI and IVIM for the uterus during the menstrual cycle that are consistent with current physiology and similar research. Therefore, DWI and IVIM can be used as techniques for human clinical research for the functional or metabolic change in the menstrual cycle based on the premise of social ethics. Second, although DWI and IVIM have been widely used in the diffuse and focal lesions of the uterus, few studies have considered changes in the menstrual cycle. We considered that the stability of the DWI and IVIM parameters in the uterus were reliable indicators for relevant studies. Because DWI and IVIM can change during the menstrual cycle, choosing an appropriate phase of the menstrual cycle for clinical research using the DWI and IVIM can ensure the relative stability of the baseline characteristics of participants; completing the relevant research during the same phase of the menstrual cycle would be more effective.

We acknowledge several limitations in our study. First, this is a single-center and small sample study. Our findings need validation through large-scale studies. Second, due to the small sample size and limited space, a subgroup analysis based on age and fertility was not applied. Third, subjective bias may exist for one observer, especially in  $D^*$  values.<sup>11,32,33</sup> Finally, although we applied enema and FOCUS technology in multiple  $b$ -value scans, artifacts from gas in the rectum or colon may still have occurred, affecting the quality of the DWI and IVIM mappings.

In conclusion, our findings demonstrate that parameters derived from ADCs and IVIM can detect differences in the uterus in diverse phases of the menstrual cycle, especially regarding ADC and  $D$  values in the endometrium, which could have a baseline impact on DWI and IVIM.

### Acknowledgments

We thank Medjaden Inc. for the scientific editing of this manuscript.

### Conflict of interest disclosure

The authors declared no conflicts of interest.

### Funding

This study was funded by the Zhuhai Medical Research Project in 2022 (2220009000170).

## References

1. Takeuchi M, Matsuzaki K, Nishitani H. Manifestations of the female reproductive organs on MR images: changes induced by various physiologic states. *Radiographics*. 2010;30(4):1147. [\[CrossRef\]](#)
2. Demas BE, Hricak H, Jaffe RB. Uterine MR imaging: effects of hormonal stimulation. *Radiology*. 1986;159(1):123-126. [\[CrossRef\]](#)
3. McCarthy S, Tauber C, Gore J. Female pelvic anatomy: MR assessment of variations during the menstrual cycle and with use of oral contraceptives. *Radiology*. 1986;160(1):119-123. [\[CrossRef\]](#)
4. Kido A, Kataoka M, Koyama T, Yamamoto A, Saga T, Togashi K. Changes in apparent diffusion coefficients in the normal uterus during different phases of the menstrual cycle. *Br J Radiol*. 2010;83(990):524-528. [\[CrossRef\]](#)
5. Kılıçkesmez Ö, Fırat Z, Oygen A, et al. Diffusion tensor imaging of the uterine zones related to the menstrual cycle and menopausal status at 3 tesla MRI. *Balkan Med J*. 2016;33(6):607-613. [\[CrossRef\]](#)
6. Li Y, Lai M, Li Q, Fu C, Zhang Q. Cyclic changes in T2\* relaxometry of human uterus during

the menstrual cycle using BOLD MR imaging. *Eur J Radiol*. 2022;156:110563. [\[CrossRef\]](#)

7. Tao YY, Zhou Y, Wang R, et al. Progress of intravoxel incoherent motion diffusion-weighted imaging in liver diseases. *World J Clin Cases*. 2020;8(15):3164-3176. [\[CrossRef\]](#)
8. Nougaret S, Horta M, Sala E, et al. Endometrial cancer MRI staging: updated guidelines of the european society of urogenital radiology. *Eur Radiol*. 2019;29(2):792-805. [\[CrossRef\]](#)
9. Jha RC, Zanella PA, Ascher SM, Rajan S. Diffusion-weighted imaging (DWI) of adenomyosis and fibroids of the uterus. *Abdom Imaging*. 2014;39(3):562-569. [\[CrossRef\]](#)
10. Inoue C, Fujii S, Kaneda S, et al. Correlation of apparent diffusion coefficient value with prognostic parameters of endometrioid carcinoma. *J Magn Reson Imaging*. 2015;41(1):213-219. [\[CrossRef\]](#)
11. Lee Y, Lee SS, Kim N, et al. Intravoxel incoherent motion diffusion-weighted MR imaging of the liver: effect of triggering methods on regional variability and measurement repeatability of quantitative parameters. *Radiology*. 2015;274(2):405-415. [\[CrossRef\]](#)
12. Meng N, Fang T, Feng P, et al. Amide proton transfer-weighted imaging and multiple models diffusion-weighted imaging facilitates preoperative risk stratification of early-stage endometrial carcinoma. *J Magn Reson Imaging*. 2021;54(4):1200-1211. [\[CrossRef\]](#)
13. Liu J, Wan Y, Wang Z, Qi Y, Qu P, Liu Y. Perfusion and diffusion characteristics of endometrial malignancy based on intravoxel incoherent motion MRI at 3.0 T: comparison with normal endometrium. *Acta Radiol*. 2016;57(9):1140-1148. [\[CrossRef\]](#)
14. Li YT, Cercueil JP, Yuan J, Chen W, Loffroy R, Wang YX. Liver intravoxel incoherent motion (IVIM) magnetic resonance imaging: a comprehensive review of published data on normal values and applications for fibrosis and tumor evaluation. *Quant Imaging Med Surg*. 2017;7(1):59-78. [\[CrossRef\]](#)
15. Satta S, Dolcianni M, Celli V, et al. Quantitative diffusion and perfusion MRI in the evaluation of endometrial cancer: validation with histopathological parameters. *Br J Radiol*. 2021;94(1125):20210054. [\[CrossRef\]](#)
16. Hu Q, Jiang P, Feng Y, et al. Noninvasive assessment of endometrial fibrosis in patients with intravoxel incoherent motion MR imaging. *Sci Rep*. 2021;11(1):12887. [\[CrossRef\]](#)
17. Zhang Q, Ouyang H, Ye F, et al. Feasibility of intravoxel incoherent motion diffusion-weighted imaging in distinguishing adenocarcinoma originated from uterine corpus or cervix. *Abdom Radiol (NY)*. 2021;46(2):732-744. [\[CrossRef\]](#)
18. Yoshimaru D, Miyati T, Suzuki Y, et al. Diffusion kurtosis imaging with the breath-

- hold technique for staging hepatic fibrosis: a preliminary study. *Magn Reson Imaging*. 2018;47:33-38. [\[CrossRef\]](#)
19. Le Bihan D, Breton E, Lallemand D, Aubin ML, Vignaud J, Laval-Jeantet M. Separation of diffusion and perfusion in intravoxel incoherent motion MR imaging. *Radiology*. 1988;168(2):497-505. [\[CrossRef\]](#)
  20. Critchley HOD, Maybin JA, Armstrong GM, Williams ARW. Physiology of the endometrium and regulation of menstruation. *Physiol Rev*. 2020;100(3):1149-1179. [\[CrossRef\]](#)
  21. Giri SK, Nayak BL, Mohapatra J. Thickened endometrium: when to intervene? A clinical conundrum. *J Obstet Gynaecol India*. 2021;71(3):216-225. [\[CrossRef\]](#)
  22. Blanks AM, Brosens JJ. Progesterone action in the myometrium and decidua in preterm birth. *Facts Views Vis Obgyn*. 2012;4(3):33-43. [\[CrossRef\]](#)
  23. Demir R, Yaba A, Huppertz B. Vasculogenesis and angiogenesis in the endometrium during menstrual cycle and implantation. *Acta Histochem*. 2010;112(3):203-214. [\[CrossRef\]](#)
  24. Dey SK, Lim H, Das SK, et al. Molecular cues to implantation. *Endocr Rev*. 2004;25(3):341-373. [\[CrossRef\]](#)
  25. Gellersen B, Brosens IA, Brosens JJ. Decidualization of the human endometrium: mechanisms, functions, and clinical perspectives. *Semin Reprod Med*. 2007;25(6):445-453. [\[CrossRef\]](#)
  26. de Ziegler D, Bulletti C, Fanchin R, Epiney M, Brioschi PA. Contractility of the nonpregnant uterus: the follicular phase. *Ann N Y Acad Sci*. 2001;943:172-184. [\[CrossRef\]](#)
  27. Salamanca A, Beltrán E. Subendometrial contractility in menstrual phase visualized by transvaginal sonography in patients with endometriosis. *Fertil Steril*. 1995;64(1):193-195. [\[CrossRef\]](#)
  28. Togashi K, Nakai A, Sugimura K. Anatomy and physiology of the female pelvis: MR imaging revisited. *J Magn Reson Imaging*. 2001;13(6):842-849. [\[CrossRef\]](#)
  29. Tan SL, Zaidi J, Campbell S, Doyle P, Collins W. Blood flow changes in the ovarian and uterine arteries during the normal menstrual cycle. *Am J Obstet Gynecol*. 1996;175(3 Pt 1):625-631. [\[CrossRef\]](#)
  30. Raine-Fenning NJ, Campbell BK, Kendall NR, Clewes JS, Johnson IR. Quantifying the changes in endometrial vascularity throughout the normal menstrual cycle with three-dimensional power Doppler angiography. *Hum Reprod*. 2004;19(2):330-338. [\[CrossRef\]](#)
  31. Bhosale P, Ramalingam P, Ma J, et al. Can reduced field-of-view diffusion sequence help assess microsatellite instability in FIGO stage 1 endometrial cancer? *J Magn Reson Imaging*. 2017;45(4):1216-1224. [\[CrossRef\]](#)
  32. Lecler A, Savatovsky J, Balvay D, et al. Repeatability of apparent diffusion coefficient and intravoxel incoherent motion parameters at 3.0 Tesla in orbital lesions. *Eur Radiol*. 2017;27(12):5094-5103. [\[CrossRef\]](#)
  33. Pieper CC, Sprinkart AM, Kukuk GM, Mürtz P. Short-term measurement repeatability of a simplified intravoxel incoherent motion (IVIM) analysis for routine clinical diffusion-weighted imaging in malignant liver lesions and liver parenchyma at 1.5T. *Rofo*. 2019;191(3):199-208. [\[CrossRef\]](#)